

---

# WATER FLOW MODEL ON VEGETATED HILLSLOPES WITH EROSION

---

A PREPRINT

Stelian Ion<sup>\*1</sup>, Dorin Marinescu<sup>†1</sup>, and Stefan-Gicu Cruceanu<sup>‡1,2</sup>

<sup>1</sup>“Gheorghe Mihoc-Caius Iacob” Institute of Mathematical Statistics and Applied Mathematics of the ROMANIAN ACADEMY, Calea 13 Septembrie No. 13, PO Box 1-24, 050711 Bucharest, Romania

<sup>2</sup>Corresponding author

August 22, 2024

## ABSTRACT

The water circulation in the Soil-Plant-Atmosphere continuum and particularly the soil erosion induced by water are problems of main concern in the new era of climate change. The present paper aims to provide a mathematical tool to investigate the water-soil and water-plant interactions involved in the complex process of water flow on plant-covered soil surfaces. Basically, the mathematical model consists of an extended Saint-Venant system of equations for water flow coupled with Hairsine-Rose equations for soil erosion. The classical Saint-Venant model is thus modified in order to take into account the presence of plants on the soil surface. On the premise that the model adequately reflects the essence of the reality, a series of numerical experiments are performed to analyze the plant induced effects on water dynamics and soil erosion intensity.

Given that both, the mathematical model and the accompanying software are flexible enough to reflect the variability of the environmental variables such as soil structure, soil surface roughness, or plant cover structure, each numerical experiment is constructed as an image of a target hydrological context. The dam break problem, flash floods, water-induced soil erosion in a catchment basin are all subjects of numerical analysis. It is shown that the presence of the plant cover drastically modifies the water dynamics and the distribution of the soil eroded particles and one can quantitatively evaluate such effects. The methods described in the paper can also help one to manage the environmental resources in order to avoid the water induced disasters.

**Keywords:** extended Saint-Venant model, porosity, numerical scheme, hydrographic basin, sediment transport, suspension, sedimentation

**MSC2020:** 76-10, 35Q35 (Primary); 76-04, 74F10, 65M08 (Secondary)

## 1 Introduction

Besides being one of the most basic and important necessities for plants, animals, and human beings, water is an essential element for life on Earth, covering about 71% of its surface. The continuous circulation of water in the Earth-Atmosphere system, the frequency and the intensity of the storms were strongly affected by the increased climate change over the last years with widespread effects on the entire environment. Knowing also that over 90% of world's disasters are weather-related (including floods, pollution, wildfire, aridification) [1], it is important for all of us to understand the hydrological cycles, to keep water in balance on earth, to proper manage the water resources in order to protect our life and material well-being. Fig. 1 illustrates a report regarding the water-related and non-water-related disasters in OECD countries [2].

---

\*ro\_diff@yahoo.com

†marinescu.dorin@ismma.ro

‡stefan.cruceanu@ismma.ro

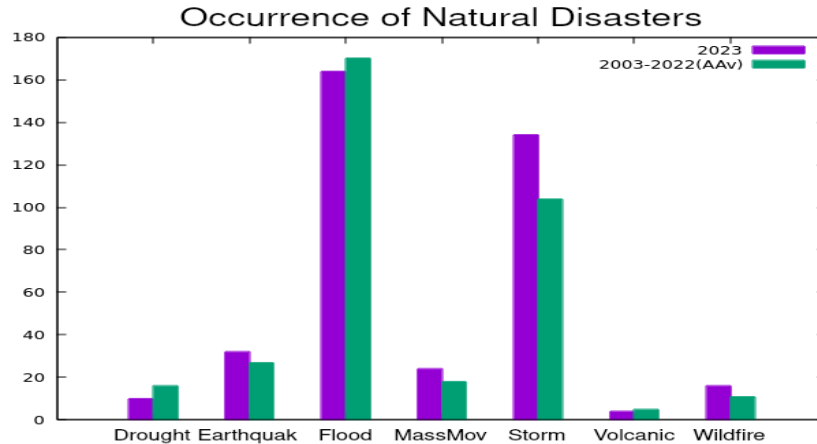


**Figure 1:** Number of water-related and non-water-related disasters in the world. Source: EM-DAT.

Problems with water distribution can be easily raised due to the nowadays increasing existence of dry or flooded areas. The dams, these barriers across the water flow, are most of the time made by humans with great purposes: to suppress floods, to provide water for human consumption, irrigation or navigability, to generate electricity, etc. The reservoirs behind these “walls” contain dangerous forces and although a dam failure is rare, it can be catastrophic, with heavy destructions on the environment as well as on the civilian population (e.g. 1975 Banqiao and Shimantan Dams, 1979 Machhu II Dam, 1985 Val di Stava Dam failures); the reader is referred to [3] for a comprehensive list of Dam Failures around the world. In this sense, having a mathematical system to model the hydrodynamic processes in a hydrographic basin and/or in a Dam Break Problem is important and needed, can help estimating the risks associated to various hazards and can provide important information regarding an economical water usage.

Before describing the model, let us say a few words about mathematical modeling and the difficulties we encounter along this process. A very brief answer to the question “What is mathematical modeling?” can be formulated as follows [4, 5]: *mathematical modeling is a cyclic process in which real-life problems are translated into mathematical language, solved within a symbolic system, and the solutions tested on real-world data.* Thus, the mathematical model is a result of the application of general principles of natural sciences, logic and mathematics. Modeling hydrological processes is a very challenging and difficult task. One can imagine for a moment the complexity of the phenomena given by the various involved watershed processes (e.g. runoff, soil erosion, precipitation, evaporation, infiltration, root uptake, plant transpiration, etc), the multitude of the factors that are involved in, only a few being quantifiable. We can add the environmental heterogeneity (diversity of vegetation and soil, variations in altitude, curvature of the soil surface etc) and it becomes obvious that we cannot take everything into account into one single model. Moreover, one can use different mathematical models for the same physical problem, depending on

- the complexity of the physical phenomena,
- the complexity of the mathematical description,
- the possibility of solving the problem (analytic, numerical),

but almost every time one must deal with the **modeller’s dilemma**:

- if the mathematical description is too complicated, then we might end up with a mathematical system with no solution;
- if the mathematical description is too simple, then we may end up not catching the essential or different aspects of the phenomenon.

Therefore, it would be ideal to use a mathematical model as simple as possible that is as suitable as possible for the physical phenomena, i.e. we do not want to kill the physical problem for the sake of mathematics. *The best models are the ones which give results closest to reality and at the same time require least number of parameters and model complexity*, [6]. We emphasize that the following minimal requirements should always hold for any mathematical model:

*solvable*      and      *physically relevant.*

The studies for models covering various hydrological applications as rainfall-runoff, flood and desertification, Dam Break Problem, echo or agricultural hydrology, etc continue to enrich the research literature. Regardless of their classification (e.g. metric, conceptual and physics-based in [6]; empirical, conceptual or physical in [7]), a model can cast into one or more classes, depending on its task, scale or structure. We mention SHE [8], MIKE-SHE [9], KINEROS [10], VIC [11], PRMS [12], SWASHES [13] among the most known physical models in hydrology.

A general physical model describing the fluid motion is given by the Navier-Stokes equations - a system of partial differential equations very difficult to treat theoretically and for which numerical approaches require huge computational effort. A simplified (derived from Navier-Stokes) and widely used version for modelling surface water flow is given by Saint-Venant equations [14]. These shallow-water equations can be slightly modified by introducing porosity in order to include the presence of the plant cover or the building distribution in urban flood studies [15, 16, 17].

It was observed that the water depth increases and its velocity decreases on a given surface soil in the presence of plants. The Saint-Venant model with porosity described later in this paper confirms these observations and thus it is feasible to use it for study the hydrological process in the presence of vegetation. Before Saint-Venant with vegetation, the previous models had considered the plants by modifying Manning's coefficient [18, 19]. Unlike these, the Saint-Venant model with vegetation highlights the effects given by the variability of the water depth and its velocity in the mass and momentum balance equations with respect to the vegetation heterogeneity.

It is known that the numerical approach to solve the porous shallow-water equations must be carefully chosen such that a good balance between the computational effort and the accuracy of the obtained solution, between the precision of the measured data and the numerical accuracy is created. Moreover, the volume of processed data and the computing effort given by high-order schemes increases excessively when working at hydrographic basin scales. In this sense, we will also briefly describe in this paper a simple discrete model based on a first-order numerical scheme with low algebraic calculations and reduced memory requirements. This is also the scheme behind our software ASTERIX for modelling the water flow on vegetated surfaces; the reader is referred to [15] for extended information. We should also mention that the model and our open-source software can be used from a laboratory or teaching level up to a hydrographic basin scale for various applications related to studying water dynamics, as

- propagation of floods produced by torrential rains,
- propagation of the flood caused by a dam break,
- studies on Riemann Problems,
- studies on the influence of plants on surface runoffs, estimating their role in the continuum Soil-Plant-Atmosphere,
- studies on landscape water flows,
- studies on vegetated bed rivers, etc.

This paper is organized as follows. In Section 2 we present the partial-differential-equation (PDE) system we use for modelling the water flow, erosion and sedimentation processes, and the numerical scheme built to approximate the solution of this model. Some numerical applications for validating both the model and the numerical method are considered in Section 3. One test is performed to compare the numerical results with the data obtained in the laboratory, while other tests (qualitative ones) are performed to emphasize the effects of vegetation, erosion and deposition processes on the asymptotic behaviour of dynamical systems defined by the numerical scheme. Section 4 presents final remarks and conclusions.

## 2 Mathematical model and numerical approximation

The model we shortly present here for water flowing over a soil surface is based on balance equations, closure empirical relations and some simplifying assumptions that do not alter the essence of the phenomena. This model couples an extended version of Saint-Venant equations (given by a mass balance and two momentum balance equations) with the Hairsine-Rose model for soil erosion and takes into account the presence of the plants on the soil surface, [15, 20].

### 2.1 Mathematical model

Assuming that the soil surface is modeled by the altitude function  $z$  defined on a bounded domain  $\mathcal{D} \subset \mathbb{R}^2$

$$x^3 = z(\mathbf{x}), \quad \mathbf{x} = (x^1, x^2) \in \mathcal{D},$$

that the sediment is partitioned into  $M$  size classes, and using Einstein summation notation, our model reads as

$$\partial_t(\theta h) + \partial_b(\theta h v^b) = \mathfrak{M}, \quad (1)$$

$$\partial_t(\theta h v^a) + \partial_b(\theta h v^a v^b) + \theta h \partial_a w = \tau_v^a + \tau_s^a, \quad (2)$$

$$\partial_t(\theta h \rho_\alpha) + \partial_b(\theta \rho_\alpha h v^b) = \theta(e_\alpha + e_\alpha^r - d_\alpha), \quad (3)$$

$$\partial_t m_\alpha = \theta(d_\alpha - e_\alpha^r), \quad (4)$$

for  $a = 1, 2$  and  $\alpha = \overline{1, M}$ , where

▷ the water depth  $h(t, \mathbf{x})$ ,

▷ the two components  $v^a(t, \mathbf{x})$  of the water velocity  $\mathbf{v} = (v^1, v^2)$ ,

▷ the mass density  $\rho_\alpha(t, \mathbf{x})$  of the suspended sediment of the size class  $\alpha$ ,

▷ the mass density  $m_\alpha(t, \mathbf{x})$  of the deposited sediment of the size class  $\alpha$

are the unknown variables. The potential  $w$  of the water level is given by

$$w(t, \mathbf{x}) = g(z(\mathbf{x}) + h(t, \mathbf{x})), \quad (5)$$

where  $g$  denotes the gravitational acceleration and  $z + h$  is the free water surface level. The flow is influenced by the presence of vegetation which is quantified by the porosity function  $\theta : \mathfrak{D} \rightarrow [0, 1]$  defined as the volume of empty space among plant stems (volume which can be filled by with water) present in a unit volume. With this notation, a bare soil is represented by

$$\theta(\mathbf{x}) = 1, \quad \forall \mathbf{x} \in \mathfrak{D}, \quad (6)$$

while a complete sealant plant cover is represented by

$$\theta(\mathbf{x}) = 0, \quad \forall \mathbf{x} \in \mathfrak{D}. \quad (7)$$

The right hand side terms  $\mathfrak{M}$ ,  $\tau_v^a$  and  $\tau_s^a$  represent the rate of water production (due to rain gain and infiltration loss) and the rates of momentum production (due to the plant cover resistance and the fluid-soil friction), respectively. The erosion and sedimentation processes are taken into account through

- $d_\alpha$  - deposition rate of the suspended sediment from the size class  $\alpha$ ,
- $e_\alpha$  - entrainment rate of the size class  $\alpha$  sediment from the soil, and
- $e_\alpha^r$  - re-entrainment rate of the size class  $\alpha$  deposited sediment, respectively.

The partial differential equations (1 - 4) of our model are quite general and we need some empirical relations in order to quantify the flow resistance due to plant and soil frictions, as well as the erosion and deposition rates.

The resistance opposed by plants to the water flow [21, 22] and the water-soil frictional forces [23] are quantified by

$$\tau_p^a = -\alpha_p h (1 - \theta) \|\mathbf{v}\| v^a, \quad \tau_s^a = -\theta \alpha_s(h) \|\mathbf{v}\| v^a, \quad (8)$$

respectively, where  $\alpha_p$  and  $\alpha_s$  are material parameters. The non-negative coefficient  $\alpha_p$  depends on the geometry of the plants from the vegetation cover, while the non-negative function  $\alpha_s(h)$  depends on the given soil surface. Some of the most used formulas for  $\alpha_s$  in the literature come from the experimental relations of Manning, Chézy, or the Darcy-Weisbach. The Darcy-Weisbach expression

$$\tau_s^a = -\theta \alpha_s \|\mathbf{v}\| v^a \quad (\text{Darcy} - \text{Weisbach}) \quad (9)$$

has the advantage of being non-singular if the water depth becomes zero.

The cumulative effects of the water-soil and water-plants interactions is assumed to be additive in this model, and we can thus introduce the resistance term

$$\tau_v^a + \tau_s^a := -\mathcal{K}(h, \theta) \|\mathbf{v}\| v^a, \quad (10)$$

where

$$\mathcal{K}(h, \theta) = \alpha_p h (1 - \theta) + \theta \alpha_s(h) \quad (11)$$

is the coefficient function of the frictional force of the water-soil-plant system.

For erosion and sedimentation processes, things are more complicated because the most of the existing data in the literature relate specifically to flows into channels or laboratory experiments. Flows on sloping surfaces have properties which are different from the ones of flows into channels, and therefore, one must work with caution when extrapolating



data from one case to another. In this article, we will use the following set of empirical relations [20, 24, 25] based on the ‘‘power stream’’ concept:

$$\begin{aligned} d_\alpha &= \nu_{s,\alpha} \rho_\alpha, \\ e_\alpha &= p_\alpha (1 - H) \frac{F(\Omega - \Omega_{cr})}{J}, \\ e_\alpha^r &= H \frac{m_\alpha}{m_t} \frac{\gamma_s}{\gamma_s - 1} \frac{F(\Omega - \Omega_{cr})}{gh}, \end{aligned} \quad (12)$$

where  $p_\alpha$  is the proportion of the sediment in size class  $\alpha$  in the original soil,

$$0 < p_\alpha \leq 1, \quad \sum_{\alpha=1}^M p_\alpha = 1$$

$\nu_{s,\alpha}$  is the settling (falling) velocity of the sediment in the size class  $\alpha$ , and  $\gamma_s$  is the relative density (with respect to water) of the sediment. The parameters  $F$  - effective fraction of power stream,  $J$  - energy of soil particles detachment and  $\Omega_{cr}$  - critical power stream are specific to a given type of soil. The erosion processes are controlled by the water flow through the stream power  $\Omega$  for which we will use the law

$$\Omega = \theta \rho_w \|\tau_s\| \|\mathbf{v}\|. \quad (13)$$

The function

$$H = \min \left\{ \frac{m_t}{m_t^*}, 1 \right\} \quad (14)$$

plays the role of a protecting factor of the original soil to the erosion process. The terms

$$m_t = \sum_{a=1}^M m_a$$

and  $m_t^*$  from (14) are the total mass of sediment deposited on the soil and the mass required to protect the original soil from erosion, respectively.

## 2.2 Numerical approximation

In what follows, we will briefly describe a numerical scheme to approximate the solution of our model (1-4). This scheme casts into the general class of methods of lines. After considering  $\{\omega_i\}_{i=\overline{1,N}}$  to be an admissible polygonal partition [26] of  $\mathcal{D}$ ,

$$\mathcal{D} = \bigcup_{i=1}^N \omega_i, \quad (15)$$

with  $\sigma_i$  being the area of the cell  $\omega_i$ , one builds a spatial discrete approximation of the model by integrating the continuous equations on each finite volume  $\omega_i$ :

$$\begin{aligned} \partial_t \int_{\omega_i} \theta h dx + \int_{\partial\omega_i} \theta h \mathbf{v} \cdot \mathbf{n} ds &= \int_{\omega_i} \mathfrak{M} dx, \\ \partial_t \int_{\omega_i} \theta h v^a dx + \int_{\partial\omega_i} \theta h v^a \mathbf{v} \cdot \mathbf{n} ds + \int_{\omega_i} \theta h \partial_a w dx &= - \int_{\omega_i} \mathcal{K} \|\mathbf{v}\| v^a dx, \quad a = 1, 2, \end{aligned} \quad (16)$$

$$\begin{aligned} \partial_t \int_{\omega_i} \theta h \rho_\alpha dx + \int_{\partial\omega_i} \theta \rho_\alpha h \mathbf{v} \cdot \mathbf{n} ds &= \int_{\omega_i} \theta (e_\alpha + e_\alpha^r - d_\alpha) dx, \\ \partial_t \int_{\omega_i} m_\alpha dx &= \int_{\omega_i} \theta (d_\alpha - e_\alpha^r) dx, \quad \alpha = \overline{1, M}, \end{aligned} \quad (17)$$

and then by defining an approximations of the integrals. Here,  $\mathbf{n} = (n_1, n_2)^T$  stands for the unit normal vector pointing towards the outside of the boundary  $\partial\omega_i$  of  $\omega_i$ . The resulting semi-discrete scheme takes the form of a system of ordinary differential equations (ODEs) written as

$$\partial_t U + \mathcal{F}(U) = \mathcal{S}(U), \quad (18)$$

where  $U$ ,  $\mathcal{F}$ , and  $\mathcal{S}$  are vectors of size  $N(3 + 2M)$ . The reader is referred to Appendix A for extended details on the explicit form of these vectors.

To obtain a numerical solution, we use a fractional time step method to integrate the ODEs. Basically, this means that we split our ODE system into two subsystems, integrate each of them and then combine the two solutions to obtain the solution of the original system. For our model, if we denote by  $\mathcal{E}^1(t)$  the evolution operator for

$$\frac{dU}{dt} = \mathcal{S}(U),$$

and by  $\mathcal{E}^2(t)$  the evolution operator for

$$\frac{dU}{dt} + \mathcal{F}(U) = 0,$$

then a first order time approximation is given by

$$U(t + \Delta t) = \mathcal{E}^1(\Delta t)\mathcal{E}^2(\Delta t)U(t), \quad (19)$$

and a second order time approximation by

$$U(t + \Delta t) = \mathcal{E}^2(\Delta t/2)\mathcal{E}^1(\Delta t)\mathcal{E}^2(\Delta t/2)U(t). \quad (20)$$

The reader is referred to Appendix B for the construction of the above two operators. It is important to mention that the time step  $\Delta t_n := t^{n+1} - t^n$  must be bounded by

$$\tau_n = CFL \frac{\phi_{\min}}{c_{\max}^n}, \quad (21)$$

due to the hyperbolic character of the shallow-water equations and to the positivity requirement of the water depth, where  $CFL$  is a number between 0 and 1 (the Courant-Friedrichs-Lewy condition) and

$$c_i = \|\mathbf{v}_i\| + \sqrt{gh_i}, \quad c_{\max} = \max_i \{c_i\},$$

$$\phi_{\min} = \min_i \left\{ \frac{\sigma_i}{\sum_{j \in \mathcal{N}(i)} l_{(i,j)}} \right\}. \quad (22)$$

Also, the following result holds:

**Theorem 1.** *For a proper definition of:*

- the flux interface term  $h_{(i,j)}(v_n)_{(i,j)}$
- the discrete gradient of the free surface  $h_{(i,j)}(w_a)_{(i,j)}$
- and the time step bound

the numerical scheme is:

- **well-balanced**,

$$\mathbf{v} = 0, h + z = ct|_{t=0} \longrightarrow \mathbf{v} = 0, h + z = ct|_{t>0}$$

- $h, \rho_\alpha, m_\alpha$  **positive scheme**

$$h > 0, \rho_\alpha > 0, m_\alpha > 0|_{t=0} \longrightarrow h > 0, \rho_\alpha > 0, m_\alpha > 0|_{t>0}$$

### 3 Numerical Applications

#### 3.1 Wave propagation through heterogeneous media

In order to better understand the Dam Break phenomena, some laboratory experiments have been designed and accomplished around the world. The experimental data were compared to theoretical results obtained using Saint-Venant equations and the reader is referred to CADAM (the European Concerted Action Project on Dambreak Modelling) project for condense knowledge and best practice on dambreak modelling. The theoretical results reported by [15, 13, 27, 28] show a good agreement with laboratory data. This fact increases the confidence in the Saint-Venant system as a mathematical model of water dynamics in the dam break phenomena. The flush flood is another important problem that deserves the attention of hydrologists. Generally, the flash food propagates in very heterogeneous

environmental media (different soil surface, plant cover or building structures). We appreciate that the vegetated Saint-Venant system (1-2) is an adequate mathematical model to study the flash flood problem. Unfortunately, there are very few experimental results concerning this problem. To help in this regard, we consider a numerical experiment where the soil surface heterogeneity is of main concern. We got inspired from the laboratory experiment in [29] consisting of a rectangular long flume partially covered by vegetation. The plant cover is uniformly distributed along the width of the flume, and therefore one deals with a 1D problem.

For our experiment, we consider a flume given by the rectangular domain

$$\mathcal{D} = \{(x, y) | 0 \leq x \leq 18, 0 \leq y \leq 5\}$$

who has two distinct complementary subdomains

$$\mathcal{D}_1 = \{(x, y) | 9 \leq x \leq 18, 2.5 \leq y \leq 5\} \quad \text{and} \quad \mathcal{D}_0 = \mathcal{D} \setminus \Omega_1$$

as pictured in Fig. 2.

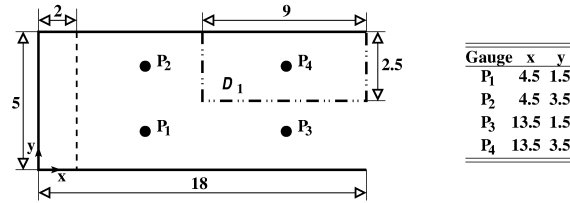


**Figure 2:** Scheme of the experimental installation for the Dam Break flow in a rectangular domain.

We assume than only  $\mathcal{D}_0$  is covered by vegetation

$$\theta = \begin{cases} \theta_1, & (x, y) \in \mathcal{D}_1 \\ 1, & (x, y) \in \mathcal{D}_0 \end{cases}$$

and/or that it has a soil surface different from the rest of the domain:

$$\alpha_s = \begin{cases} \tau_1, & (x, y) \in \mathcal{D}_1 \\ \tau_0, & (x, y) \in \mathcal{D}_0 \end{cases}$$

The boundaries of flume are considered to be impermeable walls, except the right side where we assume to have free discharge. Initially, the flume is only partially covered by water at rest

$$h(x) = \begin{cases} 1, & x \in [0, 2] \\ 0, & x \in (2, 18] \end{cases} \quad \text{and} \quad \mathbf{v} = 0.$$

This is now a 2D Riemann Problem that cannot be reduced to 1D. In order to have physical relevant parameters, the values of  $\alpha_s$  and  $\alpha_p$  are chosen by fitting [15] the experimental data from [29]. For our experiment, we slightly modify the density of cover plants and use  $\theta = 0.99$  instead of  $\theta = 0.99366$ .

The numerical results for the water depth of the flow resulting from the sudden removal of the door from  $x = 2$  are pictured in Fig. 3, Fig. 4, and Fig. 5.

Snapshots of the velocity profile at different moments of time are presented in Fig. 6.

The results show that, despite the simplicity of the configuration, the presence of heterogeneity gives rise to very complicated dynamics: water accumulation, water redistribution, backward waves (generated by the cover plant and the walls).

In the case of homogeneous soil surface, one deals with a 1D Riemann Problem which has a very simple rarefaction wave solution, see Fig. 3(d) and Fig. 5(a).

The presence of the cover plant induces:

- 1) a complicated topology of the water velocity, see Fig. 6(a-d);
- 2) water accumulation, see Fig. 6(first row) and Fig. 3(d);
- 3) water redistribution, see Fig. 5(c-d) and Fig. 6(first row);
- 4) bakward wave, see Fig. 5(e-h) and Fig. 3(a);

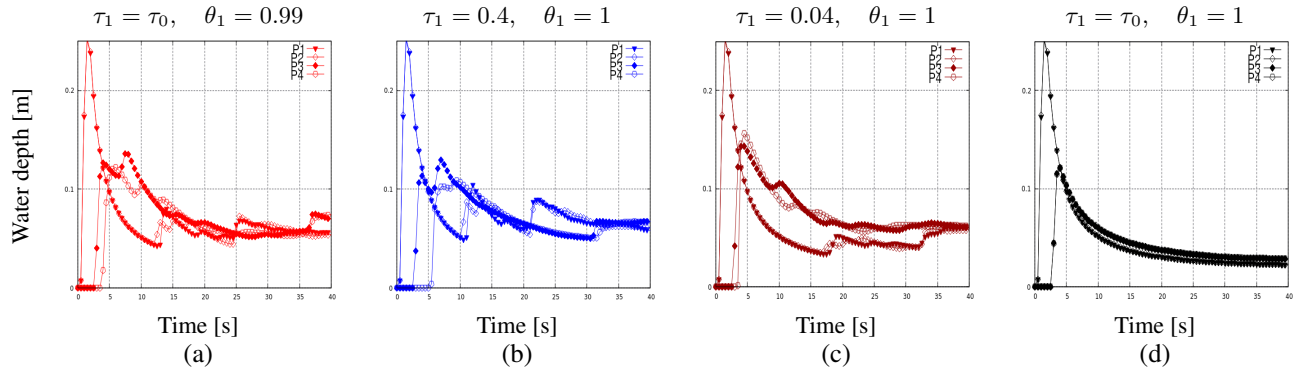


**Figure 3:** Dynamics of the water depth from the Dam Break flow at gauges P1 - P4. Each figure reveals the water depth evolution at all four gauges for the soil surface and plant cover configuration given by the values from the top row.

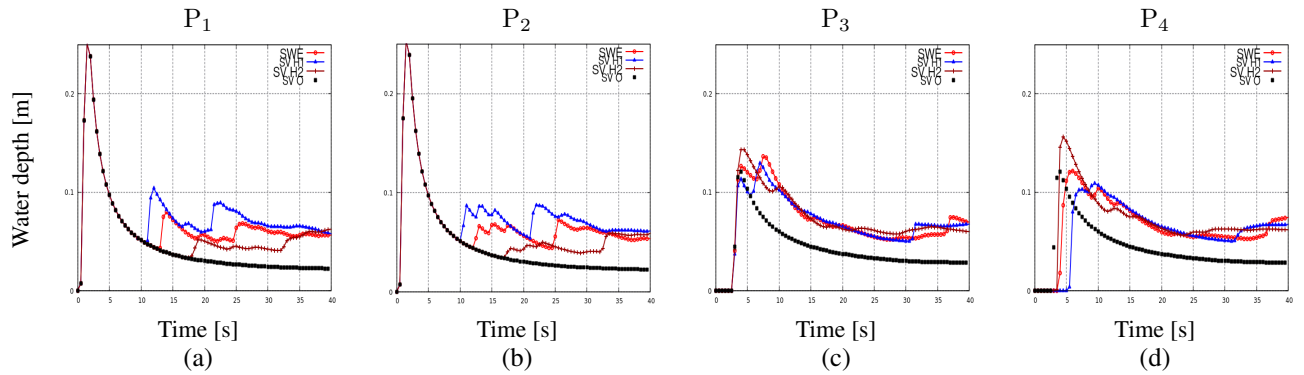


**Figure 4:** Dynamics of the water depth from the Dam Break flow at gauges P1 - P4. Each figure reveals the water depth evolution at the gauge from the top row for different soil surface and plant cover configurations.

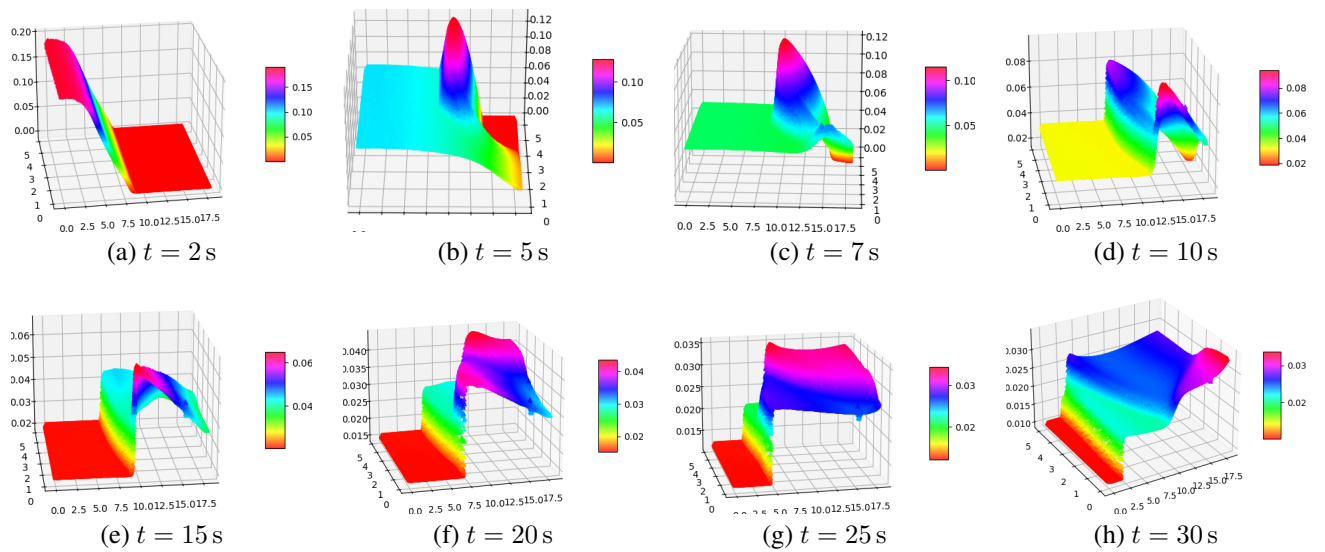


**Figure 5:** Snapshots from the water dynamics at different moments of time for the case of terrain partial covered by plants.

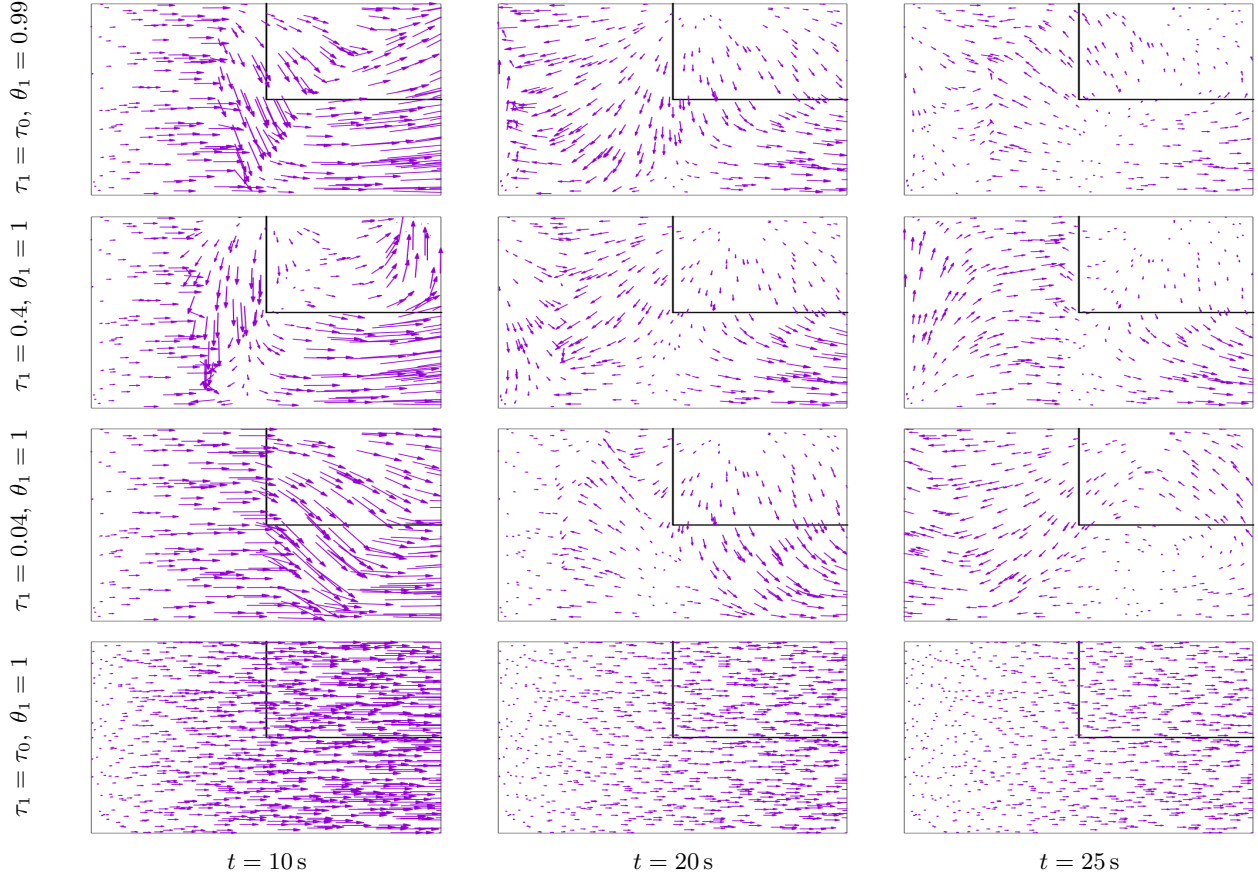


**Figure 6:** Velocity profile of the flow inside  $\mathcal{D}$  at different moments of time. The value of  $\tau_0$  from the “ambient environment”  $\Omega_0$  was kept constant for all four simulations:  $\tau_0 = 0.004$ .

5) water slowing down, Fig. 6(first row).

Also, when comparing the three simulations on the unvegetated flume ( $\theta_1 = 1$ ), one can observe that, from a qualitative point of view, significant higher water-soil frictional forces in  $\mathcal{D}_1$  (i.e. significant higher values of  $\tau_1$ ) tend to give phase portraits closer to the one given by the simulation on the partially vegetated flume ( $\theta_1 = 0.99$ ).

### 3.2 Dam Break flow in an L-shaped channel

For our next 2D simulation, we consider the CADAM test case [28] of a Dam Break flow in an L-shaped channel. The experimental installation of a reservoir feeding an impermeable channel with a  $90^\circ$  bend, its dimensions, and the location of some gauges are shown in Figure 7.

The reservoir and the channel bottom levels are set to  $z = 0$  and  $z = 0.33$  m, respectively. The boundaries are solid walls, except the far end of the channel which is considered to be free flow. Initially, the channel is dry ( $h = 0$  m) and the reservoir is filled with  $h = 0.53$  m of water at rest.

For the simulation of the **hydrodynamics**, we have some experimental data [30] on bare soil ( $\theta = 1$ ) to compare with. The flow resulting from the sudden removal of the door between the tank and the channel is complex and includes the formation of a backward wave and a reflection at the bend. These phenomena, as well as the profile of the water depth are well caught by our model, see Fig. 8.

The numerical data of the flow simulation on vegetated soil ( $\theta = 0.99$  and  $\theta = 0.97$ ) pictured on this figure show that the model can also captures the main effects of the presence of the plant cover on the Dam Break problem:

- to slow down the propagation speed of the direct wave,
- to damp the water oscillations,

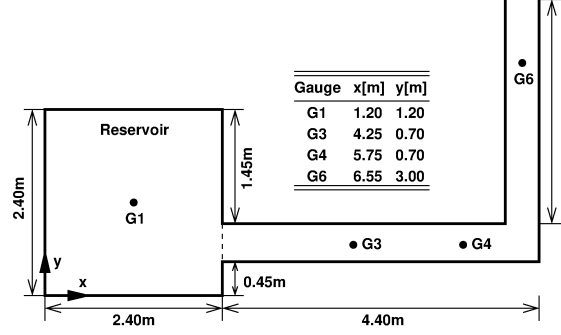


Figure 7: Scheme of the experimental installation for the Dam Break flow in an L-shaped channel.

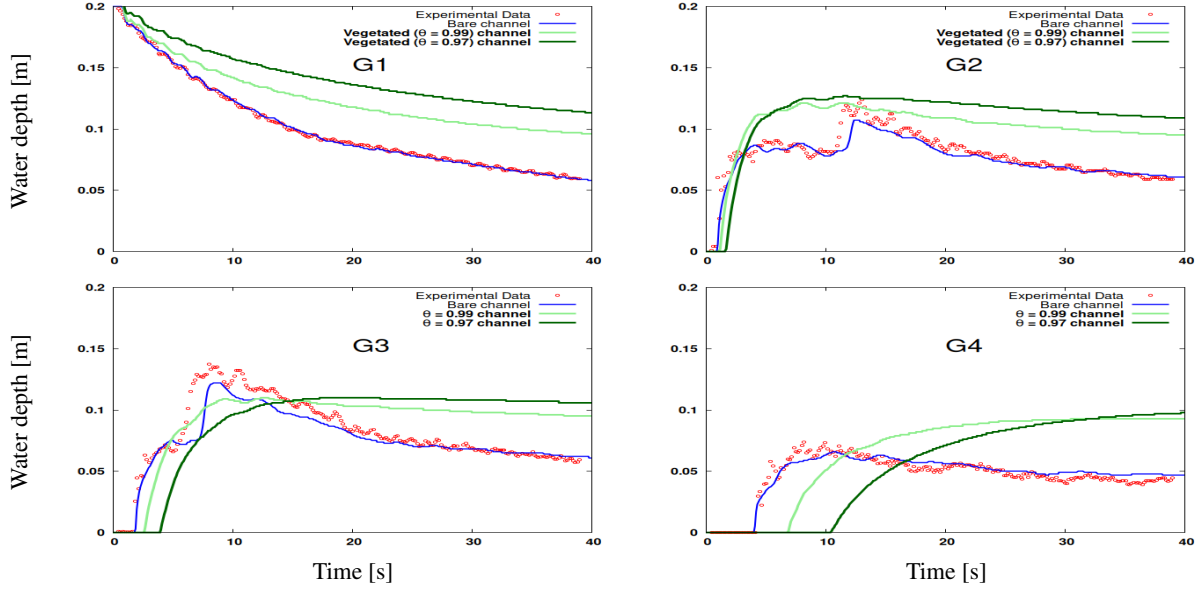


Figure 8: Dynamics of the water depth from the Dam Break flow at gauges G1 - G4: numerical data for bare and vegetated types of soil (blue and green colors, respectively) and experimental measured data (red color) for bare soil.

- the absence of backward wave.

We note that the two previous simulations (on bare and on vegetated soil surfaces) were accomplished using our software ASTERIX (which is based on the numerical scheme presented in Section 2.2) with

$$\alpha_p = 74 \text{ m}^{-1}, \quad \alpha_s = 0.002.$$

Two snapshots of the water depth and its corresponding velocity field are illustrated in Fig. 9.

We do not have any experimental data for the water flow with sediment inside such an L-shaped channel, but since the water flow module has been validated in many ways and seems to behave well, we decided to accomplish a different theoretical experiment which also includes the erosion process in order to see if the extended model (1-4) can capture its qualitative behavior.

The soil properties and the five sediment classes considered for these new simulations of the **erosion** are given in Table 1. The initial water level at rest is  $h = 0.55 \text{ m}$  inside the tank and  $h = 0.005 \text{ m}$  inside the channel, respectively. The initial values of the mass densities of the suspended and deposited sediment are considered to be 0:

$$\rho_\alpha(0) = 0, \quad m_\alpha(0) = 0, \quad \alpha = \overline{1, M}.$$

We ran ASTERIX for four simulations corresponding to two different types of vegetated soil

$$\theta = 0.98 \quad \text{and} \quad \theta = 0.96$$

and to two different values of the energy  $J$  of soil particles detachment from (12)

$$J = 5.0 \quad \text{and} \quad J = 0.1.$$

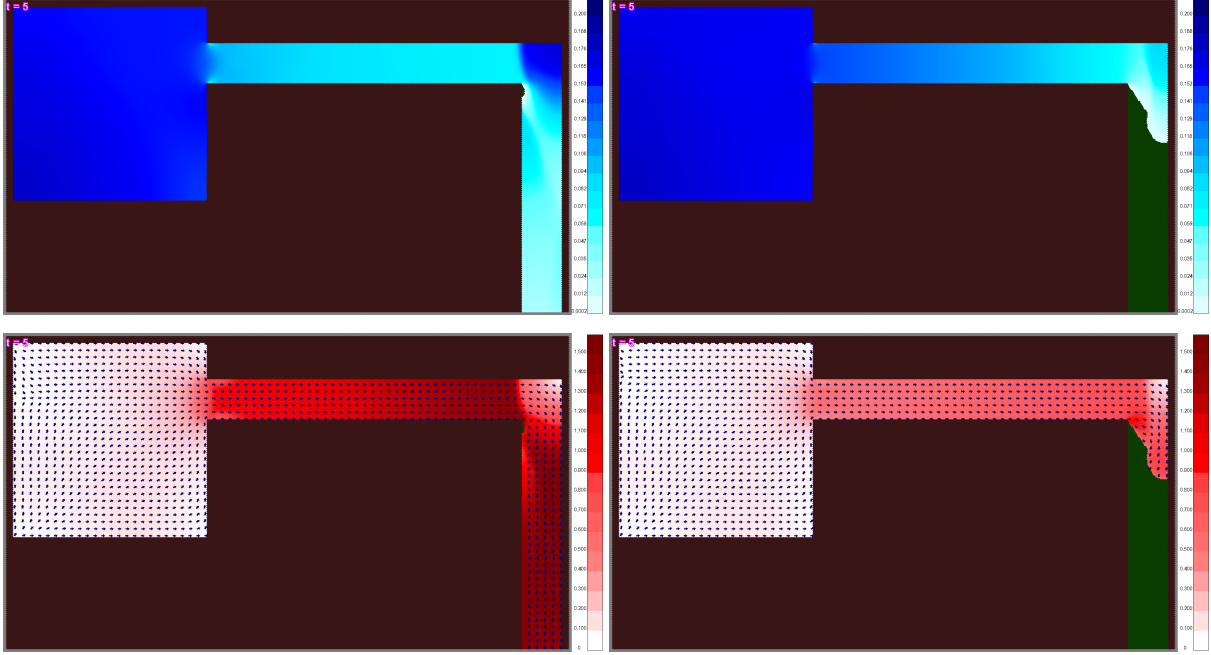


**Figure 9:** Water depth (top row, blue color gradient) and velocity distributions (bottom row, red color gradient for the modulus and arrows for the flow direction) at  $t = 5$  s for bare (left column) and vegetated (right column,  $\theta = 0.99$ ) channels.

**Table 1:** Values of the soil and sediment parameters used for the simulations on the L-shaped channel.

$\gamma_s$	$F$	$J$	$\Omega_{cr}$	$\alpha$	$p_\alpha$	$\nu_{s,\alpha}$
-	-	[J/kg]	[W/m <sup>2</sup> ]	-	-	[m/s]
				1	0.376	0.0038
				2	0.234	0.0137
2.6	0.06	5.0 & 0.1	0.007	3	0.200	0.0827
				4	0.166	0.1369
				5	0.024	0.2317

The snapshots of the mass densities  $\rho_\alpha$  and  $m_\alpha$  of the sediment in the size classes 1, 3, and 5 after  $t = 5$  s from the removal of the door between the tank and the channel are presented in Fig. 10 and Fig. 11. The concentration of the suspended sediment is represented in shades of red to blue on the top free surfaces, while the mass density of the sediment deposited on the soil is represented in shades of brown to gray at the bottom surface.

A first observation one can draw when comparing the pictures from the first to the second row in Fig 10 is that both the presence of the suspended sediment and its deposition are delayed when vegetation is denser (smaller values of  $\theta$ ). When comparing the columns, one can easily notice that the particles in larger size classes are transported more slowly and settle faster than the ones in the smaller size classes. We note the reader that the same color code legend was used for all six pictures, but it represents a scale of smaller values on the second row as compared to the ones from the first row.

When the energy  $J$  of soil particles detachment is small (**weak erosion**, see first row in Fig 11), the maximum concentration of the suspended sediment is reached closer to the tank gate as it gets heavier (as the size class of the sediment increases) and there is only a little amount of suspended sediment that is deposited faster than transported.

For higher values of the energy  $J$  of soil particles detachment (**strong erosion**, see second row in Fig 11), the maximum concentration of suspended sediment, at high values of its size, is reached further away from the tank gate. Also, the quantity of the suspended sediment in the water is higher and a part of it is deposited, but a significant part of it is also transported.

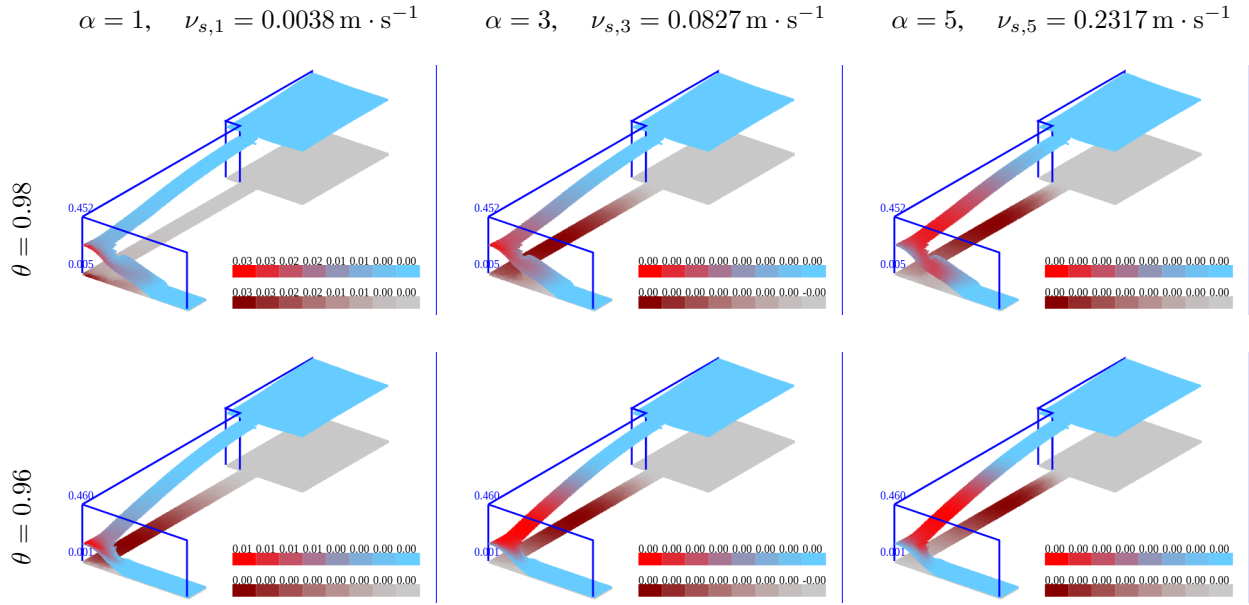


**Figure 10:** Mass densities (after  $t = 5 \text{ s}$ ) of three size classes of suspended sediment (the free surface - shades from red to blue) and of deposited sediment (the bottom surface - shades from brown to gray) found on flow simulations on two types of vegetated soil when  $J = 5.0 \text{ J} \cdot \text{kg}^{-1}$  is kept constant.

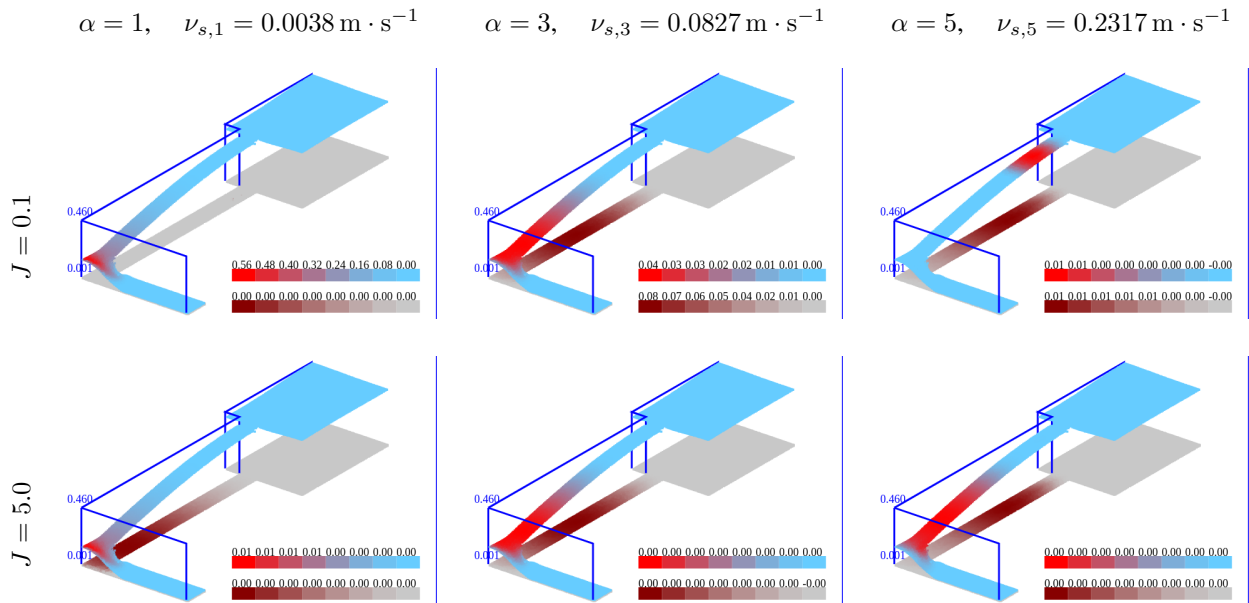


**Figure 11:** Mass densities (after  $t = 5 \text{ s}$ ) of three size classes of suspended sediment (the free surface - shades from red to blue) and of deposited sediment (the bottom surface - shades from brown to gray) found on flow simulations on the same vegetated soil  $\theta = 0.96$  for two different values of the energy  $J$  of soil particles detachment.

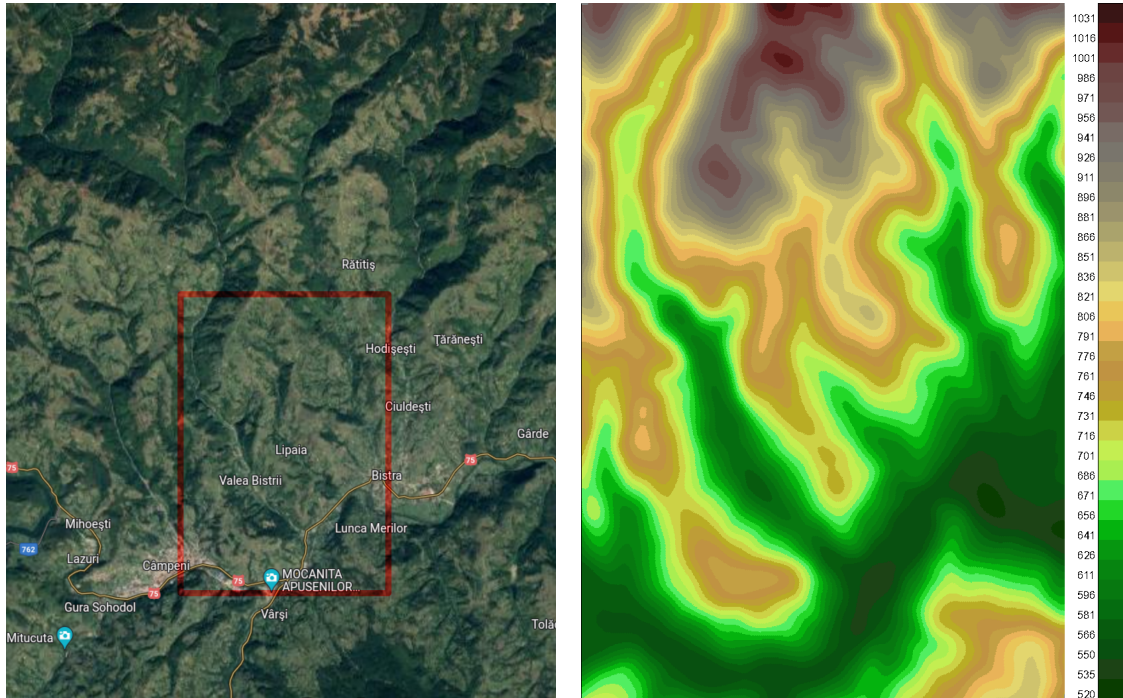


**Table 2:** Numerical output from the theoretical experiment on Lipaia's Valley. ASTERIX was run for  $t = 500$  s.

$\theta$	Water in [m <sup>3</sup> ]	Water out [m <sup>3</sup> ]	Water left [m <sup>3</sup> ]
0.999	1293921.12	87124.23	1206796.89
0.969	1293921.12	62112.39	1231808.73

### 3.3 Simulation on Lipaia's area

Lipaia is a valley in Alba County, Romania located north of Arieş River and surrounding the village (with the same name) whose geographical coordinates are  $46^\circ 23' 23''$  North,  $23^\circ 5' 19''$  East. To be closer to reality, we use the Geographic Information System (GIS) data for an approximately  $29 \text{ km}^2$  soil surface included in a  $4.50 \times 6.46 \text{ km}^2$  surrounding rectangular area, see Fig. 12. Since we do not have experimental data for plant cover density, water and

**Figure 12:** Lipaia's area. Satellite image [31] and the terrain reconstructed (from GIS data) on a hexagonal network.

velocity distributions, erosion process, we decided to accomplish the following theoretical experiment: starting with a uniform shallow water layer of 4.5 cm in depth on the entire landscape, and using two different uniform vegetation densities ( $\theta_1 = 0.999$  and  $\theta_2 = 0.969$ ), we ran our software ASTERIX on a network with 264451 hexagonal cells of radius 6.495 m to simulate the water flow across the cells for a set time interval. The hexagonal network was generated from the Lipaia's GIS raster data using the porting method introduced in [32]. For the water-plant and water-soil frictional terms (8), we considered

$$\alpha_p = 73.39 \text{ m}^{-1}, \quad \alpha_s = 0.007.$$

The water distribution at  $t = 500$  s is comparatively presented in Fig. 13 using a blue color gradient (the darkest blue corresponds to the cells with  $\theta h \geq 30h_0$ , where  $h_0 = 0.045$  m is the initial water depth). The water velocity distribution at the same moment in time is pictured in Fig. 14 using a red color gradient for the modulus of the velocity and arrows for the flow direction. The concentration of the suspended sediment is given in Fig. 15 in shades of purple and is obviously higher for the case with less vegetation. The convention of coloring the relief where  $\theta h \leq 0.1h_0$  is applied for all three figures. The sediment deposited on the ground and the eroded sediment are drawn in Fig. 16 with shades of purple and red, respectively. The data in Table 2 confirms that more water is retained in the basin if the vegetation is denser.

Furthermore, Fig. 17 emphasizes that the maximal discharge rate from the entire valley is higher and occurs earlier when vegetation is sparser.

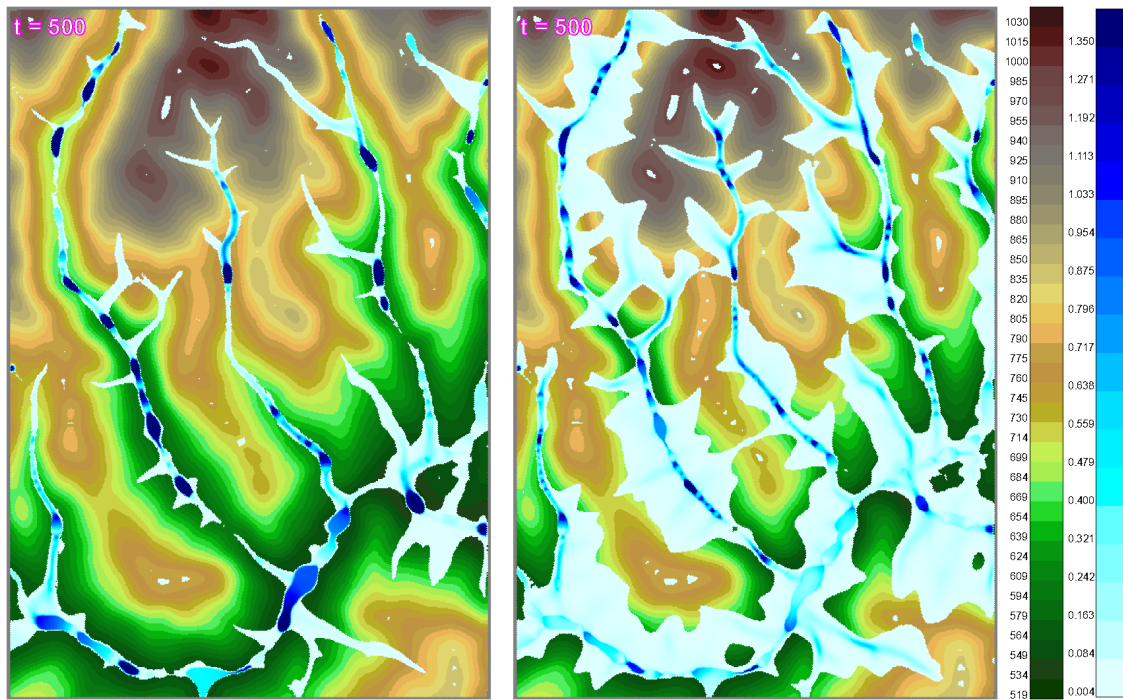


**Figure 13:** Snapshots of water distribution on Lipaia's Valley for two different uniform vegetation densities:  $\theta = 0.999$  and  $\theta = 0.969$  on the left and right picture, respectively. As expected, our numerical data are consistent with terrain observations: the amount of water leaving the basin is greater in the case of lower vegetation density.

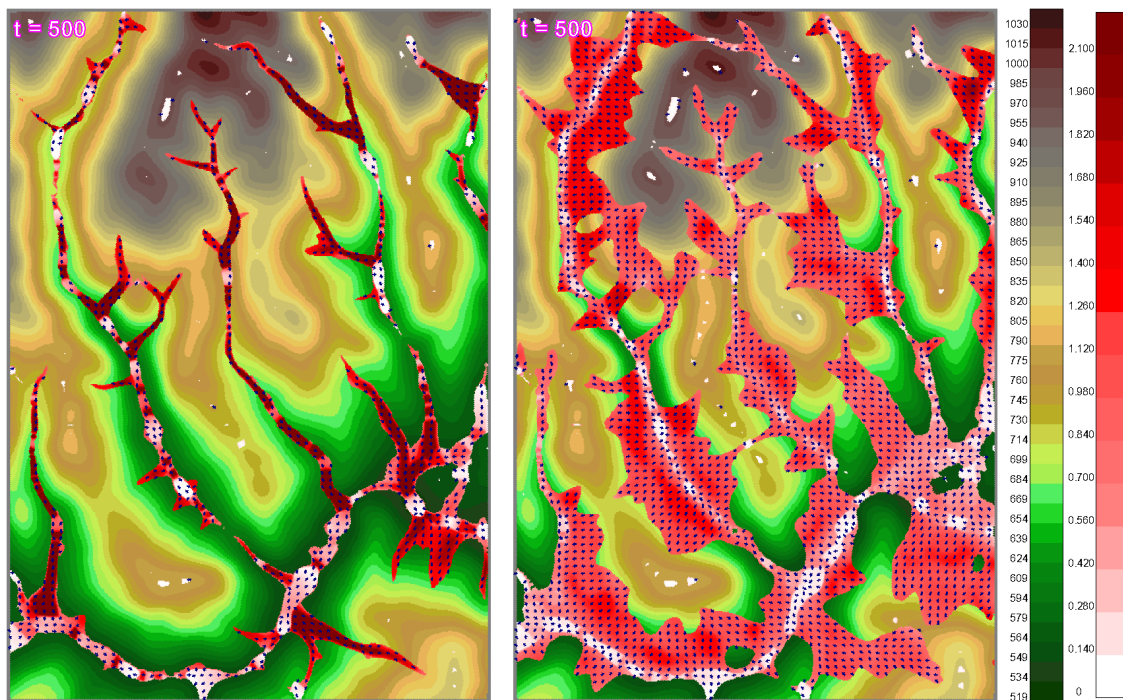


**Figure 14:** Snapshots of water velocity distribution on Lipaia's Valley for two different uniform vegetation densities:  $\theta = 0.999$  and  $\theta = 0.969$  on the left and right picture, respectively. As expected, the velocities are smaller when vegetation is denser.



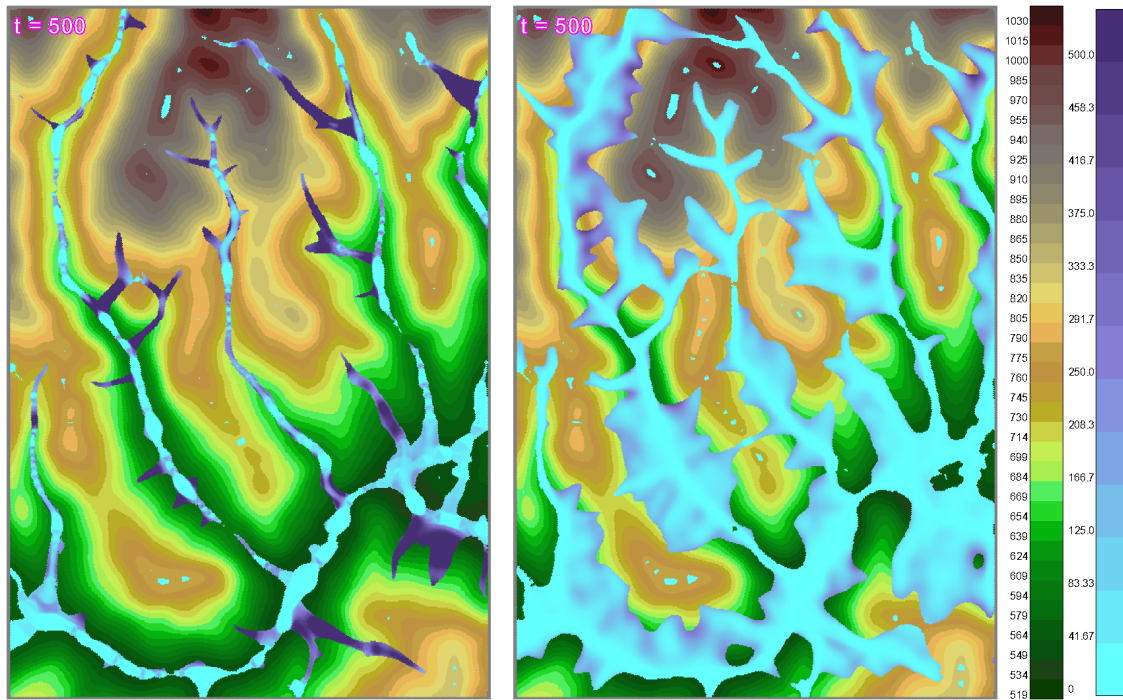


**Figure 15:** Snapshots of the concentration of the suspended sediment on Lipaia's Valley for two different uniform vegetation densities:  $\theta = 0.999$  and  $\theta = 0.969$  on the left and right picture, respectively. As expected, water is muddier when the soil is covered with less vegetation.

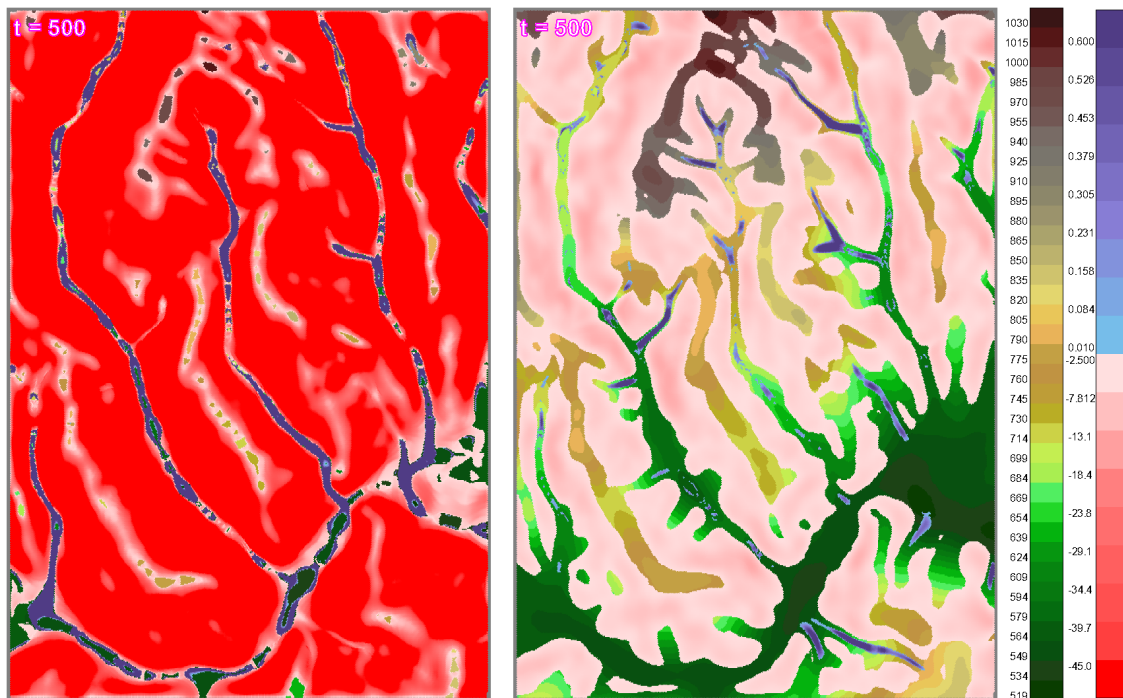


**Figure 16:** Snapshots of the sediment deposited on the ground (shades of purple) and of the eroded sediment (shades of red) on Lipaia's Valley for two different uniform vegetation densities:  $\theta = 0.999$  and  $\theta = 0.969$  on the left and right picture, respectively. It can be seen, as expected, that the erosion process is more intense when the plants are absent.

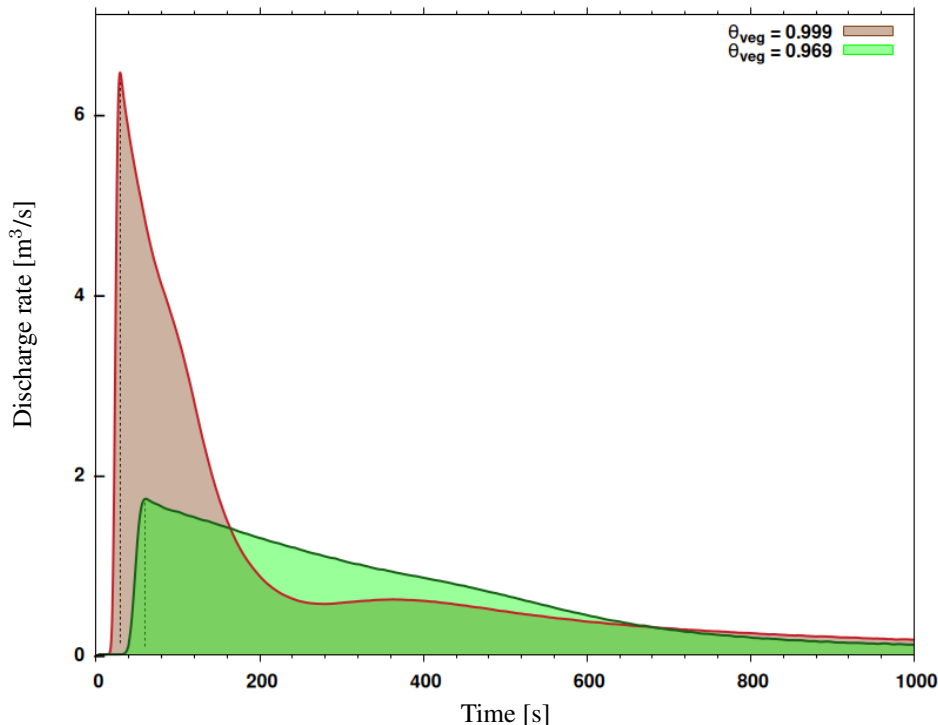


**Figure 17:** Discharge rates on Lipaia’s Valley for two different uniform vegetation densities ( $\theta = 0.969$  and  $\theta = 0.999$ ).

We note that the properties of the soil and sediment we used for the simulation on Lipaia are given in Table 3 and some snapshots from the water dynamics at four moments of time are revealed in Fig. 18.

**Table 3:** Values of the soil and sediment parameters we considered for the simulation on Lipaia’s area.

$\gamma_s$	$F$	$J$	$\Omega_{cr}$	$\alpha$	$p_\alpha$	$\nu_{s,\alpha}$
-	-	[J/kg]	[W/m <sup>2</sup> ]	-	-	[m/s]
2.6	0.2	9.0	0.09	1	0.1	0.05
				2	0.3	0.08
				3	0.6	0.25

## 4 Conclusions and Remarks

The paper focuses on a mathematical model of water and sediment dynamics on hillslopes in the presence of vegetation. The flow and erosion processes are described by balance equations and some closure empirical relations. The numerical scheme to approximate the solution of the model (1-4) is built as simple as possible in order to avoid high computational complexity, but to still be suitable to be used from a theoretical or didactic level up to practical applications on wide flow surfaces from various environmental study areas.

The paper presents three numerical experiments as prototypes of three real hydrological processes: the propagation of a flash flood in a real environment, the dam break, and the water flow and soil erosion in a catchment basin. The main goal was to illustrate the ability of the coupled extended Saint-Venant and Hairsine-Rose mathematical model and of the accompanying software to cope with various hydrological processes.

The model “affirms” that the evolution of the hydrodynamic  $(h, \mathbf{v})$  and soil erosion  $(\rho_\alpha, m_\alpha)|_{\alpha=\overline{1,M}}$  variables, collectively denoted by  $U$ , is governed by certain general principles of physics and by a set of environmental  $(z, \theta)$  and structural parameters of the soil and cover plant  $(\alpha_s, \alpha_p, F, J, \Omega_{cr}, \text{etc.})$ , collectively denoted by  $\Lambda$ . The variability of the dynamics of  $U$  is due to the variability of  $\Lambda$ . In this paper, we have shown how different values of  $\Lambda$  can be chosen to model a given hydrological process occurring in a given natural medium and how the variation in  $\Lambda$  is reflected in the variation of  $U$ .

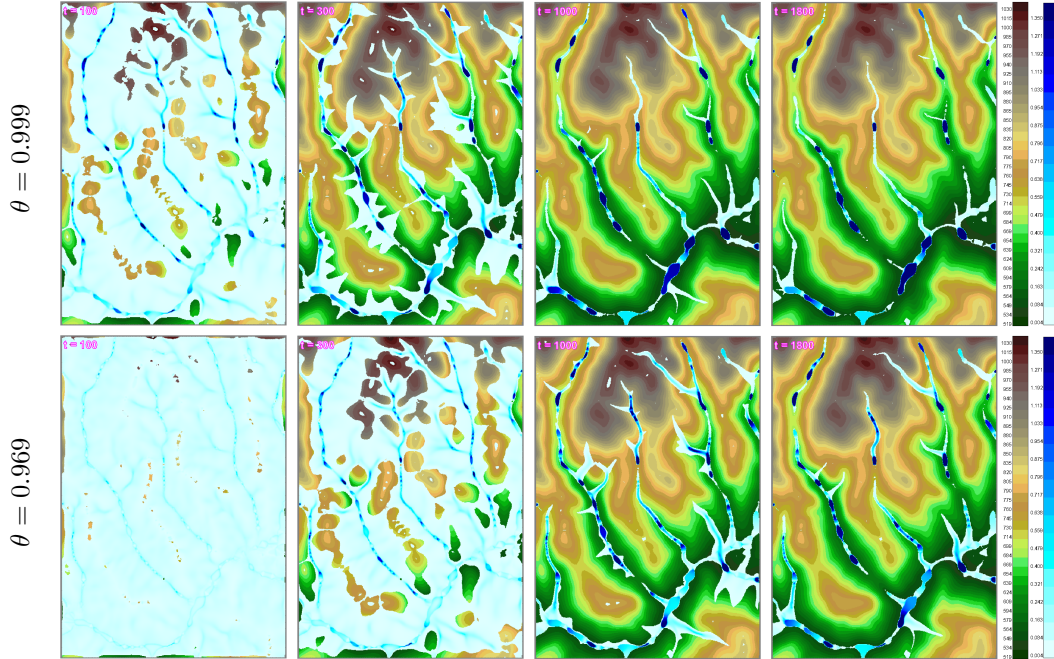


**Figure 18:** Snapshots from the water dynamics on Lipaia's basin at four moments of time: 100, 300, 1000, and 1800 s.

Before any conclusion, we must point out that the problem of soil erosion on vegetated surfaces is far from being closed by the mathematical model considered in this paper. Plant roots strongly influence the physico-chemical properties of the soil, while plant stems interact with water flow so that the parameters  $J$  related to the energy of soil particle detachment,  $F$  related to the power stream, and  $m_t^*$  related to the protection of the soil surface from erosion needs more attention.

We note here some conclusions based on the previously presented numerical results. The conclusions refer strictly to the practical application domain, those related to the mathematical area are postponed.

- In all three experiments, one observes that presence of plant cover slows down the water velocity which in turn implies a decrease in the erosion rate, see Fig. 14 and Fig. 16.
- The presence of plant or solid obstacles generates a backward wave, see Fig. 3 and Fig. 5.
- The presence of an "island of vegetation" generates a process of water accumulation in front of the island, see Fig. 3.
- Catchment areas covered with vegetation of higher density are less exposed to the flood and erosion hazards than those covered with lower density, see Figs. 15, 16 and 17.

As a final remark, we stress that the use of models based on physical processes in hydrology should be sustained and at least two arguments can be invoked in this sense:

- the increased power of mathematics to solve complicated equations and
- it is not possible to do flash flood or dam break experiments at a real scale.

We note the reader that the results of the numerical simulations considered here are obtained with ASTERIX - an open source software we have built using the "Data Porting" process described in [32] and the water flow model developed and studied in [15].

## Author Declarations

### Conflict of Interest

The authors have no conflicts to disclose.

### CRedit authorship contribution statement

All three authors contributed equally to this work: Conceptualization, Methodology, Software, Validation, Formal analysis, Data Curation, Investigation, Writing - Original Draft.

### Data Availability Statement

The data that supports the findings of this study are available within the article.

## A Explicit terms of the numerical scheme

The explicit form of the three vectors  $U$ ,  $\mathcal{F}(U)$ ,  $\mathcal{S}(U)$  from (18) for a cell  $\omega_i$  from the polygonal partition of the domain  $\mathcal{D}$  is

$$U_i = \begin{pmatrix} \theta_i h_i \\ \theta_i h_i v_i^a \\ \theta_i h_i \rho_{\alpha i} \\ m_{\alpha i} \end{pmatrix}, \quad (23)$$

$$\mathcal{F}_i = \frac{1}{\sigma_i} \begin{pmatrix} \sum_{j \in \mathcal{N}(i)} l_{(i,j)} (\theta h v_n) |_{(i,j)} \\ \sum_{j \in \mathcal{N}(i)} l_{(i,j)} (\theta h v^a v_n - \nu \Delta(v^a)) |_{(i,j)} \\ \sum_{j \in \mathcal{N}(i)} l_{(i,j)} (\theta \rho_{\alpha} h v_n) |_{(i,j)} \\ \mathbf{0}_M \end{pmatrix}, \quad (24)$$

$$\mathcal{S}_i = \begin{pmatrix} 0 \\ -\frac{1}{2\sigma_i} \sum_{j \in \mathcal{N}(i)} l_{(i,j)} w_{(i,j)}^* \widehat{\theta h}_{(i,j)} n_{\alpha} |_{(i,j)} - \mathcal{K}_i \| \mathbf{v}_i \| v_i^a \\ \theta_i e_{\alpha i} + \theta_i (e_{\alpha i}^r - d_{\alpha i}) \\ -\theta_i (e_{\alpha i}^r - d_{\alpha i}) \end{pmatrix}, \quad (25)$$

where

- $\mathbf{0}_M$  stands for the zero column vector of order  $M$ ;
- $\mathcal{N}(i)$  is the set of all cell-indexes  $j$  for which the cell  $\omega_j$  has a common side  $(i, j)$  with  $\omega_i$ ;
- $\sigma_i$  is the area of the cell  $\omega_i$ ;
- $l_{(i,j)}$  is the length of the common interface  $(i, j)$  between the cells  $\omega_i$  and  $\omega_j$ ;
- $\mathbf{n}|_{(i,j)}$  is the unitary normal to the common side of  $\omega_i$  and  $\omega_j$  pointing towards  $\omega_j$ ;
- any function  $\psi$  on a cell  $\omega_i$  is approximated by a constant value

$$\psi_i = \psi(\mathbf{x})|_{\mathbf{x} \in \omega_i}, \quad (26)$$

and hence, for example,  $h_i$  represents the value of the water depth  $h(\mathbf{x})$  on  $\omega_i$ ;

- for any common interface  $(i, j)$  between the cells  $\omega_i$  and  $\omega_j$ , the following approximations were defined:

$$\begin{aligned} (v^a)_{(i,j)} &:= \frac{v_i^a + v_j^a}{2}, \quad a = 1, 2, \\ (v_n)_{(i,j)} &:= \mathbf{v}_{(i,j)} \cdot \mathbf{n}_{(i,j)}, \\ w_{(i,j)}^* &:= w_j - w_i, \end{aligned} \quad (27)$$

$$\widehat{\theta h}_{(i,j)} := \begin{cases} \theta h_{(i,j)}, & \text{if } (v_n)_{(i,j)} \neq 0, \\ \theta_i h_i, & \text{if } (v_n)_{(i,j)} = 0 \text{ and } w_i > w_j, \\ \theta_j h_j, & \text{if } (v_n)_{(i,j)} = 0 \text{ and } w_i \leq w_j, \end{cases} \quad (28)$$

where

$$\theta h_{(i,j)} := \begin{cases} \theta_i h_i, & \text{if } (v_n)_{(i,j)} > 0, \\ \theta_j h_j, & \text{if } (v_n)_{(i,j)} < 0, \end{cases} \quad (29)$$

and

$$(\theta\rho_\alpha h)_{(i,j)} = \begin{cases} \theta_i\rho_\alpha h_i, & \text{if } (v_n)_{(i,j)} > 0, \\ \theta_j\rho_\alpha h_j, & \text{if } (v_n)_{(i,j)} < 0. \end{cases} \quad (30)$$

The dissipative term  $\nu_{(i,j)}\Delta(v^a)_{(i,j)}$  from (24) is based on the concept of artificial viscosity (see [26, 33] for example) and was introduced to improve the performance of the numerical scheme. It is given by

$$\begin{aligned} \Delta(v^a)_{(i,j)} &= v_j^a - v_i^a, \\ \nu_{(i,j)} &= \max\{c_i, c_j\} \text{med}_h(h_i, h_j), \end{aligned} \quad (31)$$

where

$$c_i = |\mathbf{v}_i| + \sqrt{gh_i}$$

and

$$\text{med}_{\theta h}(\theta_i h_i, \theta_j h_j) = \frac{2\theta_i h_i \theta_j h_j}{\theta_i h_i + \theta_j h_j}.$$

We note the reader that such an approach can be very useful for shock wave problems.

## B The evolution operators

**The construction of  $\mathcal{E}^1$ :**

- following its definition, the water depth  $h_i$  is constant and the water velocity  $\mathbf{v}_i$  can be easily evaluated independently of  $\rho_{\alpha i}$  and  $m_{\alpha i}$ ;
- for the suspended sediment variables  $\rho_{\alpha i}$ ,  $m_{\alpha i}$ , we have:

$$\begin{aligned} \frac{d(\theta_i h_i \rho_{\alpha i})}{dt} &= \theta_i e_\alpha + \theta_i (e_{\alpha i}^r - d_{\alpha i}), \\ \frac{dm_{\alpha i}}{dt} &= -\theta_i (e_{\alpha i}^r - d_{\alpha i}). \end{aligned} \quad (32)$$

For each  $i$  and each  $\alpha$ , the system (32) casts into the general form

$$\frac{dx}{dt} = r + Ax, \quad (33)$$

whose solution

$$x(t + \Delta t) = \exp(A\Delta t)x(t) + \exp(A\Delta t) \int_t^{t+\Delta t} \exp(-A(s-t)) ds r \quad (34)$$

can be approximated by

$$x(t + \Delta t) = \exp(A\Delta t)x(t) + \Delta t \exp(A\Delta t/2)r. \quad (35)$$

Here, the matrix  $A$  has the form

$$A = \begin{pmatrix} -a & b \\ a & -b \end{pmatrix} \quad (36)$$

and its exponential

$$\exp(A\Delta t)x = \begin{pmatrix} \frac{b(x_0 + y_0)}{a+b} + \exp(-(a+b)\Delta t)\frac{ax_0 - by_0}{a+b} \\ \frac{a(x_0 + y_0)}{a+b} - \exp(-(a+b)\Delta t)\frac{ax_0 - by_0}{a+b} \end{pmatrix}. \quad (37)$$

**The construction of  $\mathcal{E}^2$ :**

For the ODE system

$$\frac{dU}{dt} + \mathcal{F}(U) = 0,$$

one can easily use a Euler time step method

$$\mathcal{E}^2(\Delta t)U^0 = U^0 - \Delta t\mathcal{F}(U^0).$$

## References

- [1] United Nations Environment Programme, Disasters and climate change (2024).  
URL <https://www.unep.org/topics/fresh-water/disasters-and-climate-change>
- [2] OECD, Toolkit for Water Policies and Governance, OECD Publishing, Paris, 2021. doi:10.1787/ed1a7936-en.  
URL <https://www.oecd-ilibrary.org/content/publication/ed1a7936-en>
- [3] USBR, RCEM - Dam failure and flood event case history compilation, U.S. Department of the Interior Bureau of Reclamation.  
URL <https://www.usbr.gov/damsafety/documents/RCEM-CaseHistories2015.pdf>
- [4] C. Haines, R. Crouch, Mathematical Modelling and Applications: Ability and Competence Frameworks, Springer US, Boston, MA, 2007, pp. 417–424. doi:10.1007/978-0-387-29822-1\_46.
- [5] L. Verschaffel, B. Greer, E. de Corte, Everyday Knowledge and Mathematical Modeling of School Word Problems, Springer Netherlands, Dordrecht, 2002, pp. 257–276. doi:10.1007/978-94-017-3194-2\_16.
- [6] H. Wheeler, S. Sorooshian, K. D. Sharma, Hydrological Modelling in Arid and Semi-Arid Areas, Cambridge University Press, 2007. doi:10.1017/CB09780511535734.
- [7] J. Sitterson, C. Knightes, R. Parmar, K. Wolfe, M. Muche, B. Avant, An overview of rainfall-runoff model types, Tech. rep., U.S. Environmental Protection Agency, USA (2017).
- [8] M. Abbott, J. Bathurst, J. Cunge, P. O’Connell, J. Rasmussen, An introduction to the european hydrological system — système hydrologique européen, “she”, 1: History and philosophy of a physically-based, distributed modelling system, Journal of Hydrology 87 (1) (1986) 45–59. doi:10.1016/0022-1694(86)90114-9.
- [9] DHI, Mike she (2024).  
URL <https://www.dhigroup.com/technologies/mikepoweredbydhi/mike-she>
- [10] D. Woolhiser, R. Smith, D. Goodrich, U. A. R. Service, KINEROS: A Kinematic Runoff and Erosion Model: Documentation and User Manual, 1 disc with report, U.S. Department of Agriculture, Agricultural Research Service, ARS-77, 1989.
- [11] X. Liang, D. P. Lettenmaier, E. F. Wood, S. J. Burges, A simple hydrologically based model of land surface water and energy fluxes for general circulation models, Journal of Geophysical Research: Atmospheres 99 (D7) (1994) 14415–14428. doi:10.1029/94JD00483.
- [12] V. P. Singh, Computer Models of Watershed Hydrology, Water Resources Publications, LCC, 2012.  
URL <https://www.wrp11c.com/books/cmwhn.html>
- [13] O. Delestre, C. Lucas, P.-A. Ksinant, F. Darboux, C. Laguerre, et al., SWASHES: a compilation of shallow water analyticsolutions for hydraulic and environmental studies, International Journal for Numerical Methods in Fluids 72 (3) (2013) 269–300. doi:10.1002/flid.3741.
- [14] A. J. C. B. de Saint-Venant, Théorie du mouvement non-permanent des eaux, avec application aux crues des rivières et à l’introduction des marées dans leur lit, Comptes rendus de l’Académie des Sciences de Paris 73 (1871) 147–154, 237–240.
- [15] S. Ion, D. Marinescu, S. G. Cruceanu, Numerical scheme for solving a porous saint-venant type model for water flow on vegetated hillslopes, Appl. Numer. Math. 172 (2022) 67–98. doi:10.1016/j.apnum.2021.09.019.
- [16] G. Varra, V. Pepe, L. Cimorelli, R. Della Morte, L. Cozzolino, On integral and differential porosity models for urban flooding simulation, Advances in Water Resources 136 (2020) 103455. doi:10.1016/j.advwatres.2019.103455.
- [17] V. Guinot, A critical assessment of flux and source term closures in shallow water models with porosity for urban flood simulations, Advances in Water Resources 109 (2017) 133–157. doi:10.1016/j.advwatres.2017.09.002.
- [18] R. Manning, On the flow of water in open channels and pipes, Transactions of the Institution of Civil Engineers of Ireland 20 (1891) 161–207.
- [19] S. Bonetti, G. Manoli, C. Manes, A. Porporato, G. G. Katul, Manning’s formula and strickler’s scaling explained by a co-spectral budget model, Journal of Fluid Mechanics 812 (2017) 1189–1212. doi:10.1017/jfm.2016.863.
- [20] P. Hairsine, C. Rose, Modeling water erosion due to overland flow using physical principles: 1. sheet flow, Water Resources Research 28 (1) (1992) 237–243. doi:10.1029/91WR02380.



- [21] M. J. Baptist, V. Babovic, J. R. Uthurburu, M. Keijzer, R. E. Uittenbogaard, A. Mynett, A. Verwey, On inducing equations for vegetation resistance, *Journal of Hydraulic Research* 45 (4) (2007) 435–450. doi:10.1080/00221686.2007.9521778.
- [22] H. M. Nepf, Drag, turbulence, and diffusion in flow through emergent vegetation, *Water Resources Research* 35 (2) (1999) 479–489. doi:10.1029/1998WR900069.
- [23] H. Rouse, *Elementary Mechanics of Fluids Hardcover*, John Wiley and Sons, Inc., New York, USA, 1946.
- [24] J. Kim, V. Y. Ivanov, N. D. Katopodes, Modeling erosion and sedimentation coupled with hydrological and overland flow processes at the watershed scale, *Water Resources Research* 49 (9) (2013) 5134–5154. doi:10.1002/wrcr.20373.
- [25] G. Sander, J.-Y. Parlange, D. Barry, M. Parlange, W. L. Hogarth, Limitation of the transport capacity approach in sediment transport modeling, *Water Resources Research* 43 (2), w02403. doi:10.1029/2006WR005177.
- [26] R. L. LeVeque, *Finite Volume Methods for Hyperbolic Problems*, Cambridge University Press, Cambridge, UK, 2002.
- [27] S. Noelle, N. Pankratz, G. Puppo, J. R. Natvig, Well-balanced finite volume schemes of arbitrary order of accuracy for shallow water flows, *Journal of Computational Physics* 213 (2) (2006) 474–499. doi:10.1016/j.jcp.2005.08.01.
- [28] S. S. F. ao, Y. Zech, Dam break in channels with 90° bend, *Journal of Hydraulic Engineering* 128 (2002) 956–968. doi:10.1061/(ASCE)0733-9429(2002)128:11(956).
- [29] V. Dupuis, S. Proust, C. Berni, A. Paquier, Combined effects of bed friction and emergent cylinder drag in open channel flow, *Environmental Fluid Mechanics* 16 (6) (2016) 1173–1193. doi:10.1007/s10652-016-9471-2.
- [30] S. S. F. ao, X. Sillen, Y. Zech, Dam-break flow through sharp bends - physical model and 2d boltzmann model validation, in: *Proceedings of the CADAM meeting Wallingford, United Kingdom, March 1998; Belgium, 1999*, 1999.  
URL <https://api.semanticscholar.org/CorpusID:108737396>
- [31] Google Earth, Map of lipaia’s catchment area (2024).  
URL <https://earth.google.com/web/@46.37256484,23.0585633,703.03441311a,8667.69086094d,35y,0h,0t,0r/data=OgMKATA>
- [32] S. Ion, D. Marinescu, S. G. Cruceanu, V. Iordache, A data porting tool for coupling models with different discretization needs, *Environmental Modelling & Software* 62 (2014) 240–252. doi:10.1016/j.envsoft.2014.09.012.
- [33] A. Kurganov, G. Petrova, A second-order well-balanced positivity preserving central-upwind scheme for the Saint-Venant system, *Communications in Mathematical Sciences* 5 (1) (2007) 133–160. doi:10.4310/CMS.2007.v5.n1.a6.